CRYSTAL GROWTH & DESIGN

Article

pubs.acs.org/crystal

Improving the Solubility of 6-Mercaptopurine via Cocrystals and Salts

Lin-Lin Xu,[†] Jia-Mei Chen,*[,†] Yan Yan,[‡] and Tong-Bu Lu*[,†,‡]

[†]School of Pharmaceutical Sciences, Sun Yat-Sen University, Guangzhou 510006, China

[‡]MOE Key Laboratory of Bioinorganic and Synthetic Chemistry/State Key Laboratory of Optoelectronic Materials and Technologies/School of Chemistry and Chemical Engineering, Sun Yat-Sen University, Guangzhou 510275, China

Supporting Information

ABSTRACT: An antitumor drug, 6-mercaptopurine monohydrate, has a low oral bioavailability (about 16%) due to its poor aqueous solubility. To improve its solubility, two cocrystals of 6-mercaptopurine with 4-hydroxybenzoic acid (**1**) and 2,4-dihydroxybenzoic acid (**2**), as well as two salts with piperazine in 1:1 (**3**) and 2:1 (**4**) stoichiometry, respectively, were obtained and characterized by infrared spectra, powder and single crystal X-ray diffraction. The structures of **1**−**4** are assembled via N−H(pyrimidine)···O(carboxyl), N−H(pyrimidine)···N(imidazole), O−H(carboxyl)···S, O−H(hydroxyl)···N(imidazole), N−H(pyrimidine)···S, O−H(carboxyl)···O(carboxyl) and N−H(piperazine)···N(imidazole) hydrogen bonds. After the formation of cocrystals and salts, the solubility of 6-mercaptopurine monohydrate is much improved, and the apparent solubility values of **1**−**4** in the phosphate buffer of pH 6.8 are approximately 1.6, 2.0, 14.0, and 4.2 times as large as that of 6-mercaptopurine monohydrate. Interestingly, **3** transformed to **4** at 40 °C/75% RH within one month.

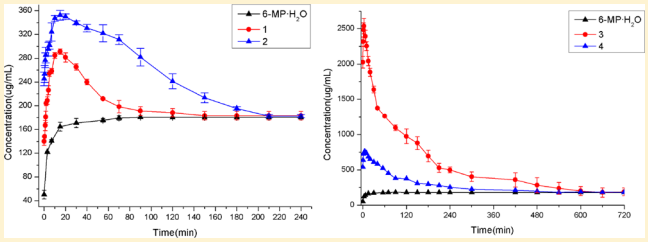

INTRODUCTION

Most drug development candidates fail to reach market due to deficient physicochemical properties, and poor aqueous solubility is recognized as the single largest physicochemical problem hindering oral drug delivery.[1] Thus solubilization of poorly soluble drugs is a very formidable task for pharmacetical scientists. Salt formation is the most common method for improving solubility and dissolution rates of acidic and basic drugs.[2] Recently, cocrystals have been identified as viable solid forms for improving the solubility of the active pharmaceutical ingredients (APIs), especially for nonionizable APIs.[3] A pharmaceutical cocrystal is defined as a stoichiometric multiple component substance formed by an API and one or more coformers, in which the API and coformers are connected by noncovalent intermolecular interactions, typically hydrogen bonds.[4−6] Therefore, the presence of hydrogen bond donors and acceptors in API and coformers is usually a precondition for cocrystal formation.[4,7] Moreover, cocrystals have been documented to be effective for modifying the physicochemical properties of an API, such as mechanical properties, melting point, hygroscopic properties, photosensitivity, dissolution behavior and bioavailability.[8−15] The versatility of cocrystals arises from the wide array of coformers. All the compounds appear on the generally regarded as safe (GRAS) or everything added to the food in the United States (EAFUS) list are potential coformers.[16]

6-Mercaptopurine (6-MP) is known as a clinically important antimetabolite and antineoplastic drug in the treatment of human leukemia, systemic lupus erythematosus, rheumatoid arthritis and inflammatory bowel disease.[17,18] The commercially available form, 6-mercaptopurine monohydrate (6-MP·H_2O), has low oral bioavailability (about 16%) due to its poor solubility in water (0.135 mg/mL).[19] Therefore, increasing the solubility of 6-MP·H_2O and consequently improving its bioavailability through preparing novel cocrystals or salts is of interest for the development of new dosage forms of 6-MP.

Scheme 1. Structures of 6-Mercaptopurine, 4-Hydroxybenzoic Acid, 2,4-Dihydroxybenzoic Acid, and Piperazine (left to right)

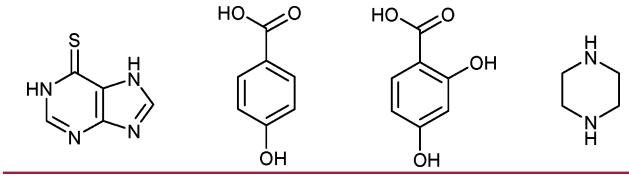

In this paper, two cocrystals of 6-MP with 4-hydroxybenzoic acid and 2,4-dihydroxybenzoic acid, and two salts of 6-MP with piperazine were obtained. 4-Hydroxybenzoic acid is listed in the GRAS substances,[20] 2,4-dihydroxybenzoic acid is enlisted in EAFUS list,[21,22] and piperazine is a pharmaceutically accepted basic salt former and has pharmacological activity as an anthelmintic.[11] All of the cocrystals and salts were characterized by infrared spectra, powder and single crystal X-ray diffraction, and their powder dissolution and stability were also investigated.

EXPERIMENTAL SECTION

Materials and General Methods. 6-MP·H_2O was purchased from Suizhou Hongqi Chemical Co., Ltd. All the coformers were purchased

Received: July 27, 2012
Revised: October 12, 2012
Published: October 31, 2012

Table 1. Crystallographic Data and Refinement Parameters for 1−4

	1	2	3	4
formula	$C_{12}H_{10}N_4O_3S$	$C_{12}H_{10}N_4O_4S$	$C_9H_{14}N_6S$	$C_{14}H_{17}N_{10}S_2$
formula weight	290.30	306.30	238.32	390.50
temperature/K	150(2)	293(2)	130(2)	150(2)
crystal system	monoclinic	monoclinic	orthorhombic	orthorhombic
space group	$P2_1/c$	$P2_1/c$	$Pbca$	$Pna2_1$
a/Å	12.3806(8)	14.3545(8)	11.0569(3)	11.4885(7)
b/Å	8.0655(6)	7.5483(4)	13.1725(3)	12.1759(6)
c/Å	12.5124(8)	12.3239(6)	15.5061(4)	12.0078(7)
α/deg	90	90	90	90
β/deg	90.292(6)	102.860(5)	90	90
γ/deg	90	90	90	90
V_{cell}/Å^3	1249.42(15)	1301.83(12)	2258.42(10)	1678.59(16)
Z	4	4	8	4
D_c/g cm^{-3}	1.543	1.563	1.402	1.545
F(000)	600	632	1008	816
crystal size/mm	0.10 × 0.10 × 0.05	0.20 × 0.10 × 0.10	0.30 × 0.30 × 0.03	0.10 × 0.05 × 0.05
index ranges	$-14 \le h \le 13$	$-16 \le h \le 17$	$-11 \le h \le 12$	$-8 \le h \le 13$
	$-9 \le k \le 8$	$-8 \le k \le 7$	$-15 \le k \le 13$	$-14 \le k \le 11$
	$-14 \le l \le 14$	$-14 \le l \le 14$	$-17 \le l \le 18$	$-14 \le l \le 10$
R_{int}	0.0291	0.0353	0.0199	0.0317
goodness-of-fit on F^2	1.042	1.101	1.051	1.014
R_1 $[I > 2\sigma(I)]$[a]	0.0602	0.0479	0.0330	0.0459
wR_2 [all data][b]	0.1566	0.1501	0.0912	0.1162
Flack parameter[c]				0.19(4)

[a] $R_1 = \Sigma||F_o| - |F_c||/\Sigma F_o$. [b] $wR_2 = [\Sigma[w(F_o^2 - F_c^2)^2]/\Sigma w(F_o^2)^2]^{1/2}$, $w = 1/[\sigma^2 (F_o)^2 + (aP)^2 + bP]$, where $P = [(F_o^2) + 2F_c^2]/3$. [c] Absolute structure parameter.[36−38]

Table 2. Hydrogen Bonding Distances and Angles for 1−4

compound	H bond	D−H/Å	H···A/Å	D···A/ Å	∠D−H···A/°
1[a]	N4−H4A···O1#1	0.94(5)	1.78(6)	2.708(4)	170(5)
	O2#1−H2A#1···S1	0.83(4)	2.38(4)	3.202(3)	169(4)
	N1#2−H1A#2···N3	0.84(5)	2.04(5)	2.846(5)	160(5)
	N1−H1A···N3#3	0.84(5)	2.04(5)	2.846(5)	160(5)
	O3−H3A···N2	0.83(4)	1.95(4)	2.768(4)	170(4)
2[b]	N1#1−H1N#1···S1	0.91(4)	2.36(4)	3.256(2)	169(3)
	N1−H1N···S1#1	0.91(4)	2.36(4)	3.256(2)	169(3)
	N4−H4N···N2#2	0.86(4)	2.17(4)	3.026(3)	172(3)
	N4#3−H4N#3···N2	0.86(4)	2.17(4)	3.026(3)	172(3)
	O1−H1A···O2#4	0.85(4)	1.81(4)	2.658(3)	175(4)
	O1#4−H1A#4···O2	0.85(4)	1.81(4)	2.658(3)	175(4)
	O3−H3A···O2	0.97(4)	1.78(4)	2.629(2)	145(3)
	O4−H4A···N3	0.86(4)	1.89(4)	2.740(3)	173(4)
3[c]	N1#1−H1#1···N4	0.91(2)	1.90(2)	2.807(2)	174(2)
	$N5^+$#2−H5B#2···N6	0.81(2)	2.16(2)	2.958(2)	169(2)
	$N5^+$−H5A···$N3^-$	0.95(2)	1.85(2)	2.790(2)	170(2)
4[d]	N5#1−H5#1···N8	0.88	2.040	2.908(4)	168.6
	$N9^+$#2−H9A#2···$N7^-$	0.92	1.900	2.782(5)	159.8
	$N10^+$#2−H10B#2···$N2^-$	0.92	1.917	2.829	170.7
	N1#3−H1A#3···N4#4	0.88	2.000	2.841	159.4

[a] Symmetry codes: #1 1 + x, −1 + y, z; #2 x, 5/2 − y; #3 x, 5/2 − y, z +1/2. [b] #1 1 − x, −y, 1 − z; #2 x, 1/2 − y, 1/2 + z; #3 x, 1/2 − y, −1/2 + z; #4 −1 − x, −y, −z. [c] #1 1/2 + x, 3/2 − y, −z + 1; #2 1/2 + x, y, 3/2 − z. [d] #1 −1/2 + x, 1/2 − y, z; #2 1 − x, 1 − y, −1/2 + z; #3 1/2 + x, 3/2 − y, z; #4 x, 1 + y, z. (D and A are hydrogen bond donors and acceptors).

from Aladdin reagent Inc. All of the other chemicals and solvents were commercially available and used as received. Elemental analyses (EA) were carried out by Elementar Vario EL elemental analyzer. The infrared spectra (IR) were recorded in the 4000 to 400 cm^{-1} region using KBr pellets and a Bruker EQUINOX 55 spectrometer. Thermogravimetric analyses (TGA) were recorded on a Netzsch TG-209 instrument and platinum crucible in nitrogen atmosphere, with a heating rate of 10 °C/min.

6-MP/4-Hydroxybenzoic Acid Cocrystal (1:1), 1. This cocrystal was prepared via the following two methods: (i) A mixture of 6-MP·H_2O (34.0 mg, 0.2 mmol) and 4-hydroxybenzoic acid (27.6 mg, 0.2 mmol) was added to 2 mL of methyl acetate and allowed to stir for 2 days at 50 °C. The suspension was filtered and the isolated solid of **1** was dried under a vacuum for 24 h at ambient temperature. Yield: 50.8 mg, 82.5%. The filtrate was left to evaporate slowly at room temperature in a sealed glass

dx.doi.org/10.1021/cg3010745 | Cryst. Growth Des. 2012, 12, 6004−6011

Scheme 2. Hydrogen Bonds in the Structure of 6-MP·H_2O (left), and Possible Hydrogen Bonding Synthons (I–IV) of 6-MP with Coformers (right)

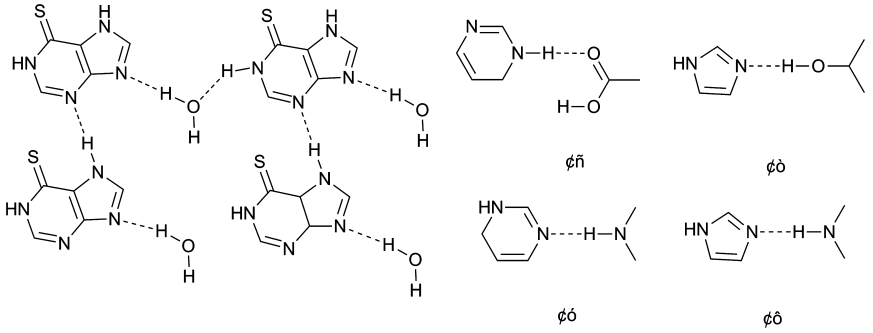

desiccator containing P_2O_5. After 4 days, block-shaped crystals of **1** were obtained. (ii) A 1:1 mixture of 6-MP·H_2O (170.2 mg, 1.0 mmol) and 4-hydroxybenzoic acid (138.1 mg, 1.0 mmol) was added to stainless steel grinding jar. Approximately two drops of ethanol was added, and the mixture was ground for 30 min at a frequency of 20 Hz. Anal. (%) Calcd for $C_{12}H_{10}N_4O_3S$: C, 49.47; H, 3.47; N, 19.30; S, 11.05. Found: C, 49.45; H, 3.58; N, 19.30; S, 11.03. IR data (KBr, cm^{-1}): 3015, 2813, 1669, 1618, 1589, 1382, 1256, 1166, 1156, 881, 772, 614, 528.

6-MP/2,4-Dihydroxybenzoic Acid Cocrystal (1:1), 2. This cocrystal was prepared via the following two methods: (i) A mixture of 6-MP·H_2O (34.0 mg, 0.2 mmol) and 2,4-dihydroxybenzoic acid (30.8 mg, 0.2 mmol) was added to 2 mL of methanol and allowed to stir for 2 days at 50 °C. The suspension was filtered and the isolated solid of **2** was dried under a vacuum for 24 h at ambient temperature. Yield: 56.5 mg, 87.2%. The filtrate was left to evaporate slowly at room temperature in a sealed glass desiccator containing P_2O_5. After 2 days, block-shaped crystals of **2** were obtained. (ii) A 1:1 mixture of 6-MP·H_2O (170.2 mg, 1.0 mmol) and 2,4-dihydroxybenzoic acid (154.1 mg, 1.0 mmol) was added to stainless steel grinding jar. Approximately two drops of ethanol was added, and the mixture was ground for 30 min at a frequency of 20 Hz. Anal. (%) Calcd for $C_{12}H_{10}N_4O_4S$: C, 47.05; H, 3.29; N, 18.29; S, 10.47. Found: C, 46.88; H,3.39; N, 18.22; S, 10.41. IR data (KBr, cm^{-1}): 3047, 2914, 1643, 1623, 1566, 1351, 1255, 1179, 1017, 981, 847, 793, 621, 591, 481.

6-MP/Piperazinium Salt (1:1), 3. This salt was prepared via the following two methods: (i) 6-MP·H_2O (50.0 mg, 0.3 mmol) was added to a nearly saturated solution of piperazine (100.0 mg, 1.2 mmol) in methanol (1 mL) and allowed to stir for 2 days at 50 °C. The suspension was filtered and the isolated solid of **3** was dried under a vacuum for 24 h at ambient temperature. Yield: 53.2 mg, 35.5%. The filtrate was left to evaporate slowly at room temperature in a sealed glass desiccator containing P_2O_5. After 5 days, rod-shaped crystals of **3** were obtained. (ii) A 1:1 mixture of 6-MP·H_2O (170.2 mg, 1.0 mmol) and piperazine (86.1 mg, 1.0 mmol) was added to stainless steel grinding jar. Approximately two drops of ethanol was added, and the mixture was ground for 30 min at a frequency of 20 Hz. Anal. (%) Calcd for $C_9H_{14}N_6S$: C, 45.36; H, 5.92; N, 35.26; S, 13.46. Found: C, 45.41; H, 5.80; N, 34.94; S, 13.34. IR data (KBr, cm^{-1}): 3230, 1587, 1374, 1180, 1113, 1011, 852, 666, 573, 462, 416.

6-MP/Piperazinium Salt (2:1), 4. A mixture of 6-MP·H_2O (170.2 mg, 1.0 mmol) and piperazine (43.0 mg, 0.5 mmol) was added to 6 mL of ethanol and allowed to stir for 2 days at 50 °C. The suspension was filtered and the isolated solid of **4** was dried under a vacuum for 24 h at ambient temperature. Yield: 181.9 mg, 85.3%. The filtrate was left to evaporate slowly at room temperature within a sealed glass desiccator containing P_2O_5. After about 15 days, block-shaped crystals of **4** were obtained. Anal. (%) Calcd for $C_{14}H_{17}N_{10}S_2$: C, 43.17; H, 4.40; N, 35.96; S, 16.47. Found: C, 43.11; H, 4.44; N, 35.94; S, 16.45. IR data (KBr, cm^{-1}): 3143, 1595, 1457, 1408, 1376, 1325, 1196, 1118, 995, 854, 654, 516, 424.

Single Crystal X-ray Diffraction. Diffraction data for crystals **1**, **2**, and **4** were collected using an Agilent Technologies Gemini A Ultra system, and diffraction data for **3** were collected on an Agilent Xcalubur Nova CCD diffractometer, with Cu Kα radiation (λ = 1.5418 Å). Data reduction and cell refinement were performed with the program of CrysAlis PRO.[23] The structures were solved by the direct method using the SHELXS-97 programs[24] and refined by the full-matrix least-squares method on F^2. All non-hydrogen atoms were refined with anisotropic displacement parameters. One 6-MP anion in **4** is disordered, which was refined with an occupancy ratio of 70:30. The positions of hydrogen atoms on nitrogen and oxygen atoms in **1**–**3** were located in Fourier-difference electron density maps; all the other hydrogen atoms were placed in calculated positions with fixed isotropic thermal parameters and included in the structure factor calculations in the final stage of full-matrix least-squares refinement. Crystal data and details of refinements of **1**–**4** are listed in Table 1, and the hydrogen bonding distances and angles are given in Table 2.

X-ray Powder Diffraction (XRPD). Room and variable temperature XRPD data were obtained on a Bruker D8 Advance with Cu Kα radiation (40 kV, 40 mA). Each sample was scanned between 5 and 40° (2θ) with 0.02° 2θ step size and 0.12 s/step scan speed. Experimental XRPD patterns were compared to XRPD patterns simulated from the single crystal data of **1**–**4**.

Powder Dissolution Experiments. Concentrations of **1**–**4** and 6-MP·H_2O in the phosphate buffer of pH 6.8 were determined by a Cary 50 UV spectrophotometry, and the absorbance values were related to solution concentrations using a calibration curve. The solids were milled to powders and sieved using standard mesh sieves to provide samples with approximate particle size ranges of 75–150 μm. In a typical experiment, 100 mL of phosphate buffer (pH 6.8) was added to a flask containing 300 mg of sample, and the resulting mixture was stirred at 25 °C and 500 rpm. At each time interval an aliquot of the slurry was withdrawn from the flask and filtered through a 0.22 μm nylon filter. And appropriate dilutions were made to maintain absorbance readings within the standard curve. The resulting solution was measured with a UV/vis spectrophotometer. After the dissolution experiment, the remaining solids were collected by filtration, dried and analyzed by XRPD, and the pH values of the resulting solutions were also measured.

Stability Test. Stability was evaluated at 40 °C/75% RH. Vial of each sample was subjected to the condition for one month. Then the samples were immediately analyzed by XRPD.

RESULTS AND DISCUSSION

To evaluate the potential for cocrystallization, the structure of 6-MP·H_2O was analyzed in terms of the available hydrogen bond donors and acceptors. In the structure of 6-MP·H_2O,[25] 6-mercaptopurine molecules are connected by water molecules via two hydrogen bonds of N–H(pyrimidine)···O(water) and O–H(water)···N(imidazole) to form a 1D chain, and the adjacent chains are further linked by N–H(imidazole)···N(pyrimidine) hydrogen bonds to generate a 2D structure (Scheme 2). So 6-mercaptopurine has potential to form hydrogen bonds (Scheme 2) with compounds containing carboxylic, hydroxyl and amino groups, etc. Therefore, a series of coformers

dx.doi.org/10.1021/cg3010745 | Cryst. Growth Des. 2012, 12, 6004–6011

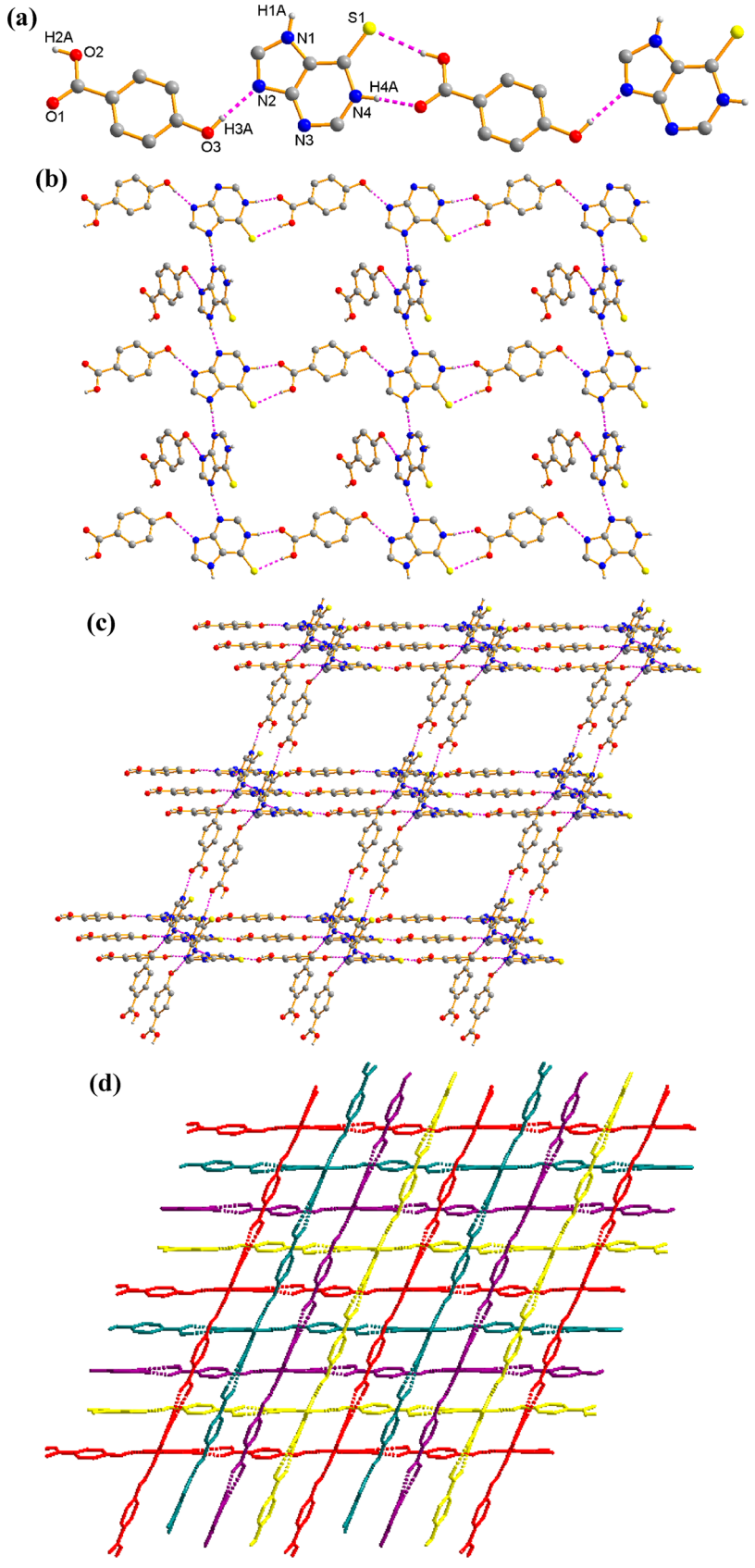

Figure 1. (a) 1D chain, (b) a crossover mode among 1D chains, (c) 3D framework with 1D channels, and (d) four-folded interpenetrating in **1**.

containing such groups were used to screen cocrystals with 6-mercaptopurine monohydrate, and two cocrystals and two salts were obtained.

Crystal Structures. The asymmetric unit of **1** contains one 6-MP and one 4-hydroxybenzoic acid molecules. As shown in Figure 1a, 4-hydroxybenzoic acid molecules alternately connect

dx.doi.org/10.1021/cg3010745 | *Cryst. Growth Des.* 2012, 12, 6004−6011

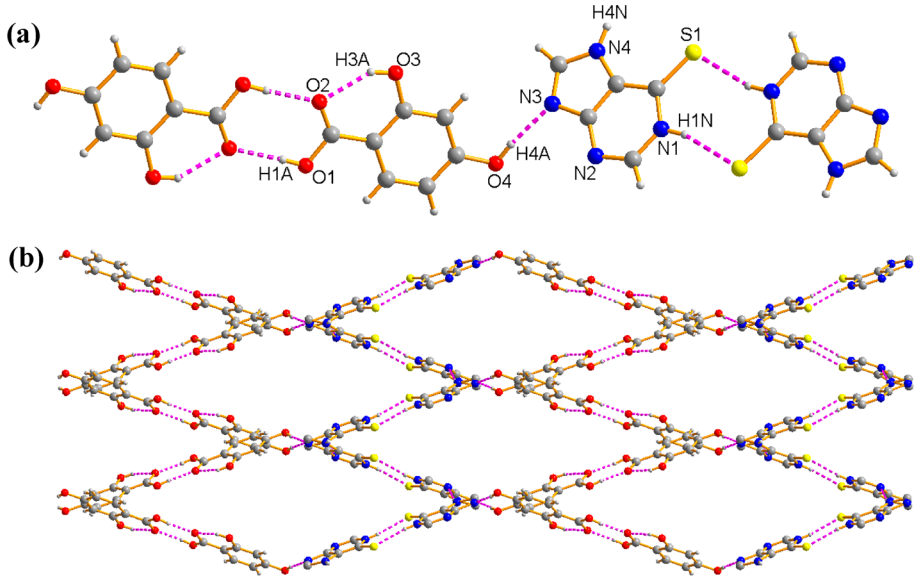

Figure 2. (a) 1D zigzag chain, and (b) 3D structure in **2**.

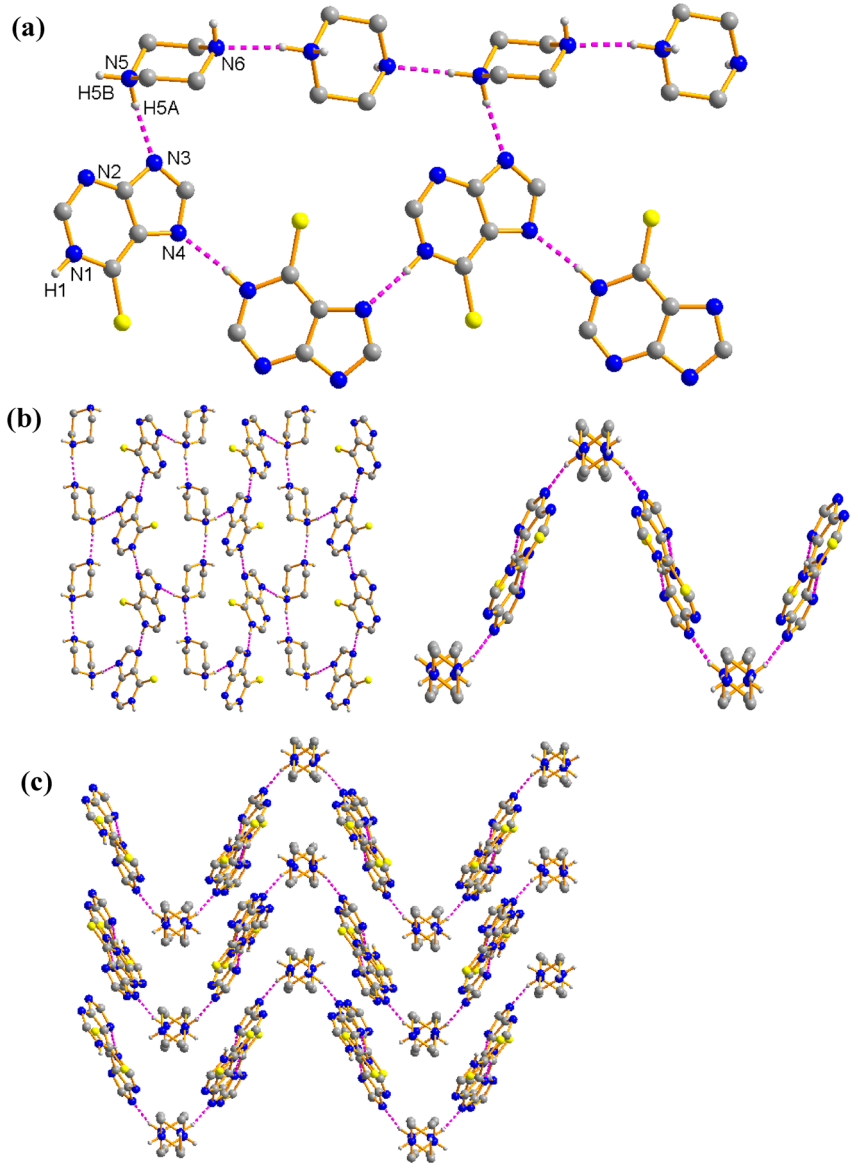

Figure 3. (a) 1D chain, (b) side view (left) and front view (right) of 2D sheet, (c) 3D structure in **3**.

dx.doi.org/10.1021/cg3010745 | *Cryst. Growth Des.* 2012, 12, 6004−6011

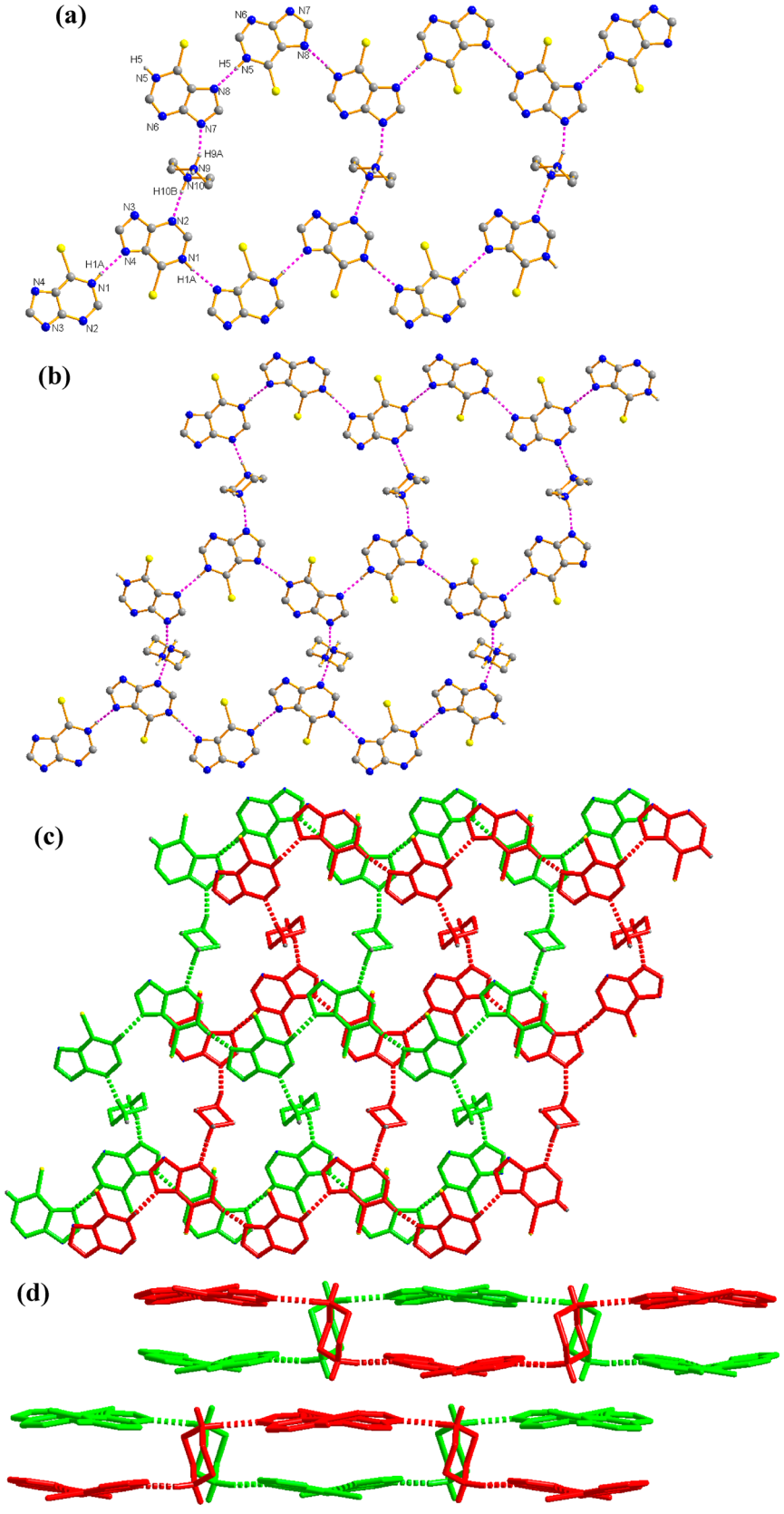

Figure 4. (a) Two 1D anion chains of 6-MP connected by piperazinium cations in **4**. (b) The 2D sheet. (c) A two-folded interpenetrating 2D bilayer. (d) The 3D structure of **4**.

6-MP molecules with three hydrogen bonds of N4−H4A···O1, S1···H2A-O2 and O3−H3A···N2 to form a one-dimensional (1D) chain. The 1D chains are further connected in a crossover mode through N1−H1A···N3 hydrogen bonds (Figure 1b) to generate a three-dimensional (3D) framework (Figure 1c) with 1D channels; the sizes of the channels are 16.13 × 24.76 Å.

dx.doi.org/10.1021/cg3010745 | *Cryst. Growth Des.* 2012, 12, 6004−6011

Because of the large void of the 1D channels in **1**, the 3D frameworks are four-folded interpenetrating[26] to generate the structure of **1** (Figure 1d).

Similar to **1**, the asymmetric unit of **2** also contains one 6-MP and one 2,4-dihydroxybenzoic acid molecule. As shown in Figure 2a, two 2,4-dihydroxybenzoic acid molecules form a dimer through two O2···H1A-O1 intermolecular hydrogen bonds. Two 6-MP molecules in **2** also form a dimer through two S1···H1N−N1 intermolecular hydrogen bonds. Two dimers are alternately linked through N3···H4A-O4 intermolecular hydrogen bonds to generate a 1D zigzag chain (Figure 2a). The 1D chains are held together by N4−H4N···N2 hydrogen bonds to generate the 3D structure of **2** (Figure 2b).

The asymmetric unit of **3** contains one 6-MP anion and one piperazinium cation, in which a proton is transferred from the imidazole group of 6-MP to the nitrogen atom of piperazine. As shown in Figure 3a, all the 6-MP anions form a 1D anion chain through intermolecular N4···H1−N1 hydrogen bonds, all the piperazinium cations also form a 1D cation chain through N6···H5B−$N5^+$ hydrogen bonds. The 6-MP anion chains alternately connect the piperazinium cation chains through charged-assisted hydrogen bonds[27−30] of $N3^-$···H5A−$N5^+$ to form a 2D wave-like sheet (Figure 3b). The 2D wave-like sheets are further held together through intersheet $\pi\cdots\pi$ interactions to form the 3D structure of **3** (Figure 3c), with the centroid···centroid distance[31] of 4.23 Å.

In contrast to **3**, the asymmetric unit of **4** contains two 6-MP anions and one piperazinium cation, in which two protons are transferred from two imidazole groups of two 6-MP molecules to two nitrogen atoms of one piperazine molecule. As shown in Figure 4a, the 6-MP anions are separately linked by intermolecular hydrogen bonds of N8···H5−N5 and N4···H1A−N1 to form two 1D chains. The adjacent 1D chains are further connected by piperazinium cations through two charged-assisted hydrogen bonds[27−30] $N9^+$−H9A···$N7^-$ and $N10^+$−H10B···$N2^-$ to generate a 2D sheet (Figure 4b). The 2D sheets are two-folded interpenetrating[26] to form a 2D bilayer (Figure 4c), and the 2D bilayers are further connected by the interlayer $\pi\cdots\pi$ interactions to generate the 3D structure of **4** (Figure 4d), with a centroid··· centroid distance[31] of 4.267 Å.

XRPD Analyses and Powder Dissolution Studies. XRPD was used to check the crystalline phase purity of **1**−**4.** The results show that the patterns of the products are different from either that of 6-MP·H_2O or those of corresponding coformers (Figure S1), indicating the formation of new crystalline phases, and all the peaks displayed in the measured patterns for **1**−**4** closely match those in the simulated patterns generated from single-crystal diffraction data (Figure S1), confirming the single phases of **1**−**4** were formed, and the isolated solids **1**−**4** are the same forms as the single crystals.

Dissolution rate and apparent solubility of solids are of paramount importance in pharmaceutical development and quality control, and shorter dissolution times and higher apparent solubility may result in more absorption. Powder dissolution profiles for 6-MP·H_2O and **1**−**4** in phosphate buffer of pH 6.8 are shown in Figure 5. It can be found that **1**−**4** show an increase in the dissolution rate and solubility values. Compounds **1** and **2** reach a maximum solubility (S_{max}) within 15−20 min, while **3** and **4** reach S_{max} after 5 min, and then decrease over the time. This specific type of profile is a product of the "spring and parachute effect" which has been exhibited by many pharmaceutical cocrystals.[32−35] The maximum solubility values for **1**, **2**, **3** and **4** are approximately

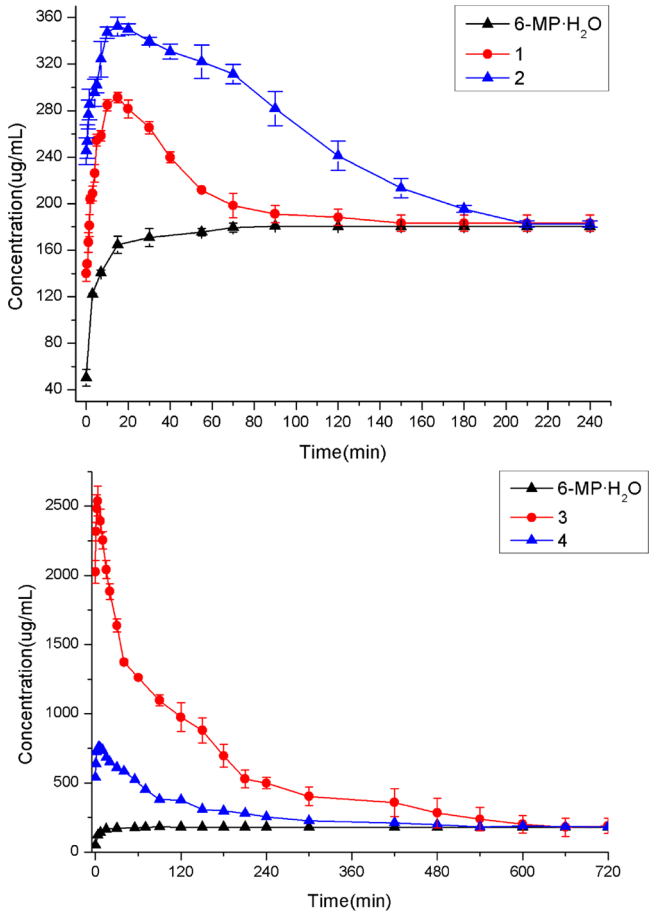

Figure 5. Powder dissolution profiles for 6-MP·H_2O and **1**−**4** in the phosphate buffer of pH 6.8.

1.6, 2.0, 14.0, and 4.2 times as large as that of 6-MP·H_2O. The pH values of the resulting solutions for **1**−**4** and 6-MP·H_2O after the powder dissolution experiments were measured, and no significant pH change was observed. The undissolved solids were filtered and dried under a vacuum, and the results of XRPD analyses indicate **1**−**4** transformed to 6-MP·H_2O (Figure S2).

Stability. Since **1**−**4** transformed to 6-MP·H_2O during the powder dissolution experiments, the cocrystals and salts may also give rise to solid-state physical stability concerns. Consequently, the stability of **1**−**4** at 40 °C/75% RH was also monitored for one month. The results of XRPD measurements indicate that **1**, **2** and **4** remained their initial crystal form, while **3** converted to **4** (Figure S3). This means that **4** is more stable than **3** at 40 °C/75% RH. The strong volatility of piperazine is a major reason for the transformation from **3** to **4**.

The results of TGA also demonstrate that **4** is more stable than **3**. The TGA curves of **3** and **4** show a weight loss starting at 142 and 173 °C, respectively (Figure S4); the weight loss of 33.0% between 142 and 181 °C for **3** is consistent with the loss of one piperazine molecule (calcd 33.1%), and the weight loss of 22.0% between 173 and 207 °C for **4** is consistent with the loss of half piperazine molecule (calcd 22.1%). Variable temperature XRPD was used to monitor the transition from **3** to **4** (Figure 6). The XRPD patterns of **3** show that **3** maintains its crystallinity up to 140 °C, and then it transforms to the mixture of **4** and 6-MP at 145 °C and completely transforms to 6-MP at 155 °C.

dx.doi.org/10.1021/cg3010745 | *Cryst. Growth Des.* 2012, 12, 6004−6011

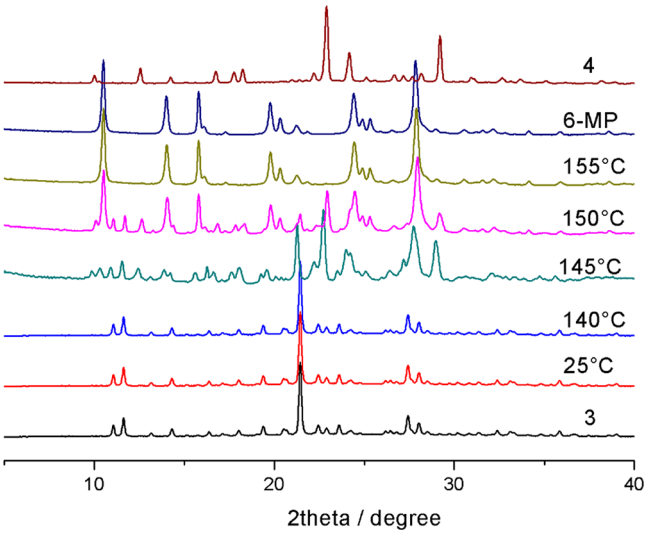

Figure 6. Variable temperature XRPD of **3**.

CONCLUSIONS

Two cocrystals of 6-MP with 4-hydroxybenzoic acid (**1**) and 2,4-dihydroxybenzoic acid (**2**), as well as two salts of 6-MP with piperazine in 1:1 (**3**) and 2:1 (**4**) stoichiometry, were synthesized, and their structures were determined by single crystal X-ray diffraction. The structures of **1**−**4** are assembled via intermolecular hydrogen bonds. The solubility of 6-MP·H_2O has been increased after the formation of **1**−**4**, indicating the solubility of 6-MP·H_2O can be improved via cocrystals and salts. **1**−**3** can be stable at 40 °C/75% RH for over one month, while **3** transformed to **4**.

ASSOCIATED CONTENT

Supporting Information

The XPRD patterns for **1**−**4** and TGA curves for **1** and **2**. This material is available free of charge via the Internet at http://pubs.acs.org.

AUTHOR INFORMATION

Corresponding Author

*Fax: +86-20-84112921. E-mail: chenjm37@mail.sysu.edu.cn (J.-M.C.); lutongbu@mail.sysu.edu.cn (T.-B.L.).

Notes

The authors declare no competing financial interest.

ACKNOWLEDGMENTS

This work was supported by 973 Program of China (2012CB821705), NSFC (91127002, 21121061, 20831005 and 21101173).

REFERENCES

(1) Stahl, P. H.; Wermuth, C. G. *Handbook of Pharmaceutical Salts: Properties, Selection, and Use*; Wiley-VCH: Zurich, 2011.
(2) Serajuddin, A. T. M. *Adv. Drug Delivery Rev.* **2007**, *59*, 603−616.
(3) Stevens, J. S.; Byard, S. J.; Schroeder, S. L. M. *J. Pharm. Sci.* **2010**, *99*, 4453−4457.
(4) Rehder, S.; Löbmann, M. K. A. M.; Strachan, C. J.; Sakmann, A.; Gordon, K.; Rades, T.; Leopold, C. S. *Pharmaceutics* **2011**, *3*, 706−722.
(5) Shan, N.; Zaworotko, M. J. *Drug Discovery Today* **2008**, *13*, 440−446.
(6) Aakeröy, C. B.; Champness, N. R.; Janiak, C. *CrystEngComm* **2010**, *12*, 22−43.
(7) Fleischman, S. G.; Kuduva, S. S.; McMahon, J. A.; Moulton, B.; Bailey Walsh, R. D.; Rodríguez-Hornedo, N.; Zaworotko, M. J. *Cryst. Growth Des.* **2003**, *3*, 909−919.
(8) Ghosh, S.; Bag, P. P.; Reddy, C. M. *Cryst. Growth Des.* **2011**, *11*, 3489−3503.
(9) Trask, A. V.; Motherwell, W. D. S.; Jones, W. *Cryst. Growth Des.* **2005**, *5*, 1013−1021.
(10) Vangala, V. R.; Chowa, P. S.; Tan, R. B. H. *CrystEngComm* **2011**, *13*, 759−762.
(11) Bethune, S. J.; Schultheiss, N.; Henck, J. *Cryst. Growth Des.* **2011**, *11*, 2817−2823.
(12) Zheng, S. L.; Chen, J. M.; Zhang, W. X.; Lu, T. B. *Cryst. Growth Des.* **2011**, *11*, 466−471.
(13) Smith, A. J.; Kavuru, P.; Wojtas, L.; Zaworotko, M. J.; Shytle, R. D. *Mol. Pharmaceutics* **2011**, *8*, 1867−1876.
(14) Karki, S.; Friscic, T.; Fabian, L.; Laity, P. R.; Day, G. M.; Jones, W. *Adv. Mater.* **2009**, *21*, 3905−3909.
(15) Yan, Y.; Chen, J. M.; Geng, N.; Lu, T. B. *Cryst. Growth Des.* **2012**, *12*, 2226−2233.
(16) Arora, K. K.; Tayade, N. G.; Suryanarayanan, R. *Mol. Pharmaceutics* **2011**, *8*, 982−989.
(17) Wang, C. C.; Chiou, S. S.; Wu, S. M. *Electrophoresis* **2005**, *26*, 2637−2642.
(18) Kato, Y.; Matsushita, T.; Yokoyama, T.; Mohri, K. *Pharm. Res.* **1992**, *9*, 697−699.
(19) Zacchigna, M.; Cateni, F.; Luca, G. D.; Drioli, S. *Bioorg. Med. Chem. Lett.* **2007**, *17*, 6607−6609.
(20) Lakshmi Kumar, T.; Vishweshwar, P.; Moses Babu, J.; Vyas, K. *Cryst. Growth Des.* **2009**, *9*, 4822−4829.
(21) Lemmerer, A.; Bernstein, J.; Kahlenberg, V. *CrystEngComm* **2010**, *12*, 2856−2864.
(22) Sander, J. R.; Bucar, D. K.; Henry, R. F.; Zhang, G. G.; MacGillivray, L. R. *Angew. Chem., Int. Ed.* **2010**, *49*, 7284−7288.
(23) *CrysAlis*^{Pro} Version 1.171.35.19;. Agilent Technologies Inc.: Santa Clara, CA, USA, 2011.
(24) Sheldrick, G. M. *Acta Crystallogr. A* **2008**, *64*, 112−122.
(25) Brown, G. M. *Acta Crystallogr. B* **1969**, *25*, 1338.
(26) Baburin, I. A.; Blatov, V. A.; Carlucci, L.; Ciani, G.; Proserpio, D. M. *CrystEngComm* **2008**, *10*, 1822−1838.
(27) Draškovic, B. M.; Bogdanovic, G. A.; Neelakantan, M. A.; Chamayou, A. C.; Thalamuthu, S.; Avadhut, Y. S.; Schmedt auf der Günne, J.; Banerjee, S.; Banerjee, S.; Janiak, C. *Cryst. Growth Des.* **2010**, *10*, 1665−1676.
(28) Wu, B.; Huang, X; Xia, J.; Y, Z.; Yang, X. J.; Janiak, C. *CrystEngComm* **2007**, *9*, 676−685.
(29) Dorn, T.; Janiak, C.; Abu-Shandi, K. *CrystEngComm* **2005**, *7*, 633−641.
(30) Ward, M. D. *Chem.Commun.* **2005**, 5838−5842.
(31) Janiak. *C. J. Chem. Soc., Dalton Trans.* **2000**, 3885−3896.
(32) Takata, N.; Takano, R.; Uekusa, H.; Hayashi, Y.; Terada, K. *Cryst. Growth Des.* **2010**, *10*, 2116−2122.
(33) Stanton, M. K.; Tufekcic, S.; Morgan, C.; Bak, A. *Cryst. Growth Des.* **2009**, *9*, 1344−1352.
(34) Takata, N.; Takano, R.; Uekusa, H.; Hayashi, Y.; Terada, K. *Cryst. Growth Des.* **2008**, *8*, 3856−3862.
(35) Cheney, M. L.; Shan, N.; Healey, E. R.; Hanna, M.; Wojtas, L.; Zaworotko, M. J.; Sava, V.; Song, S.; Sanchez-Ramos, J. R. *Cryst. Growth Des.* **2010**, *10*, 394−405.
(36) Flack, H. D.; Sadki, M.; Thompson, A. L.; Watkin, D. J. *Acta Crystallogr. A* **2011**, *67*, 21−34.
(37) Flack, H. D.; Bernardinelli, G. *Chirality* **2008**, *20*, 681−690.
(38) Flack, H. D.; Bernardinelli, G. *Acta Crystallogr. A* **1999**, *55*, 908−915.